Wave function mapping conditions in Open Quantum Dots structures

M. Mendoza and P. A. Schulz

Instituto de Física Gleb Wataghin, UNICAMP, Cx.P. 6165, 13083-970, Campinas, SP, Brazil

We discuss the minimal conditions for wave function spectroscopy, in which resonant tunneling is the measurement tool. Two systems are addressed: resonant tunneling diodes, as a toy model, and open quantum dots. The toy model is used to analyze the crucial tunning between the necessary resolution in current-voltage characteristics and the breakdown of the wave functions probing potentials into a level splitting characteristic of double quantum wells. The present results establish a parameter region where the wavefunction spectroscopy by resonant tunneling could be achieved. In the case of open quantum dots, a breakdown of the mapping condition is related to a change into a double quantum dot structure induced by the local probing potential. The analogy between the toy model and open quantum dots show that a precise control over shape and extention of the potential probes is irrelevant for wave function mapping. Moreover, the present system is a realization of a tunable Fano system in the wave function mapping regime. PACS number(s) 73.40.Gk,73.21.Fg,73.21.La

I. INTRODUCTION

Experimental probing of electronic states in systems showing spatial quantization is probably the most direct visualization of quantum mechanical effects. Such probing in condensed matter has been a challenge over decades until the development of artificial model structures, initially semiconductor quantum wells and more recently quasi one (or zero) dimensional mesoscopic systems. The control over the design and fabrication of these structures lead naturally to the introduction of well defined local probes of the electronic states. A landmark in the wavefunction spectroscopy is the optical probing of quantum-well eigenstates by Marzin and Gerard more then ten years ago [1]. The basic idea introduced in this work is that a very thin barrier, which can therefore be considered as a delta function, is grown within the quantum well at a certain position, leading to a potential perturbation of the form $V\delta(z - z_0)$. Such perturbation probes the probability density at z_0 by means of the eigenvalues, E_i, shifts, which in first-order approximation are simply:

$$E_i^{'} = E_i + V|\Psi_i(z_0)|^2 \qquad (1)$$

In the work by Marzin and Gerard, these energy shifts were obtained by photoluminescence measurements performed in a set of nominally identical quantum wells but with the perturbative barrier located at different positions. In other words, such mapping rely on measurements performed on different samples, each one probing the wave function at a designed position. Later on, Salis and coworkers [2] performed a wave function spectroscopy on a single parabolic quantum well, where the electron distribution was displaced with respect to a fixed perturbative barrier by applying an electric field. The energy shifts were obtained now by magnetotransport measurements. The great advantage of this procedure, namely the spectroscopy on a single sample, is somehow eclipsed by the fact that only a specific system (parabolic quantum wells) is suitable for it. A variation of this spectroscopy is the introduction of monolayers with magnetic ions embedded in different positions of a quantum well, using the Zeeman spliting as a probe for the wave function [3]. An alternative approach, based on energy shifts measured by means of resonant tunneling, has been proposed also a few years ago [4]. Now the mapping of the probability density along the quantum well is related to shifts of the resonant tunneling current peaks for an ensemble of double barrier tunneling diodes, where each sample has a perturbative potential spike located at a specific position. This tunneling wavefunction spectroscopy has not yet been experimentaly verified. Nevertheless, magneto-tunneling has been used as a tool for imaging of electron wave functions in self-assembled quantum dots [5].

Imaging of wave functions, in spite of the efforts mentioned above, has experienced a growing interest mainly due to the use of scanning probe microscopes in searching local electron distributions in mesoscopic systems. Within an already long list of achievements, it is worth mentioning the study of Bloch wave functions in quasi one dimensional systems, such as single wall carbon nanotubes [6] and imaging of bound states in quantum corrals [7]. In both cases scanning tunneling microscopes were used. Closely related to the approaches using perturbative potential spikes are the use of atomic force microscopes with the measurement of shifts in the conductance across a mesoscopic system as a function of the position of the potential perturbation induced by the tip of the AFM. An interesting application of this method is the imaging of coherent electron flow from a Quantum Point Contact [8].

In the present work we analyse the suitability of such imaging procedure for quasi-bound states in open quantum dot system in the resonant tunneling regime. It can be considered the two-dimensional counterpart of the probing of quasi bound states in double-barrier quantum wells, considered as a toy model. We are here mainly interested in the conditions that maximize the energy shift of the resonances in the transmission probability, with-

out breaking the perturbative regime within the mapping of the wave function can be established. In the present situation we are dealing with the quasi-bound states of a double point contact in the resonant tunneling regime, a rather different situation than single quantum point contacts [8], theoretically discussed within a similar framework [9]. Although our main concern is the mapping of quantum dot states, related to resonance shifts in energy, the analysis could also be extended to the behavour of the transmission probability plateaus related to the quantum point contact channels [10].

An important point in the present work is that, if a wave function mapping could be experimentally achieved, the open quantum dot system coupled to an AFM tip would be a realization of a tunable Fano system. Fano resonances have been recently observed in electronic transport through a single-electron transistor [11], but a tunability of the effect has been reached only in the presence of magnetic fields [12], with the quantum dot in an Aharonov-Bohm interferometer. The degree of freedom introduced by the movable AFM tip opens a new possibility for such tuning in the absence of magnetic field effects. Although Fano resonances have been discussed before in the context of mesoscopic systems, the present work proposes a possible experimental realization of former theoretical predictions [13].

II. WAVE FUNCTION IMAGING IN A TOY MODEL

The wavefunction mapping in double-barrier resonant tunneling devices is our toy model to discuss how far can a resonant transmission probability peak be shifted, within a simple approach that contains the essential features related to the problem. The coherent transmission probability is calculated in the effective-mass approximation for a double-barrier structure with an embeded perturbative barrier, as a function of electron incident energy [14]. Having in mind $GaAs/Al_xGa_{1-x}As$ structures [15], the double-barrier potential profile, considering the conduction band Γ minimum, is illustrated in the inset of Fig.1(a). The relevant parameters are the ratio between barrier heights, H/V_b; and the ratio between characteristic widths, L/L_W. Examples of transmission probabilities as a function of incident electron energy are shown in Fig. 1(a).

The use of potential spikes at controled positions as a mapping tool for the probability density inside a double-barrier resonant tunneling diode has a severe limitation in the resolution of the energy shifts obtained from rather broad current-density voltage characteristics peaks. On the other hand, increasing the energy shift of a quantum well resonance has an intrinsic upper bound. As an example for the lowest state, this upper bound is achieved when the energy shift $\Delta E_1 = E_1' - E_1$, as a function of

spike position z_0, is comparable to the energy difference ΔE_{12}, between the lowest two quasi-bound states of the system.

The evolution of the energy shift is illustrated in Fig. 1(a) for a quantum well $L_W = 150\mathring{A}$ wide. The probing potential spike is at the center of the structure with $H/V_b = 1$ and $L \leq 30\mathring{A}$. The lowest two resonances of a unperturbed double-barrier quantum well is set as a reference (thin continuous line). Energy shifts due to spikes one and three monolayers thick (dashed line, $L = 3\mathring{A}$, and long-dashed line , $L = 10\mathring{A}$, respectively) show the same qualitative features. Having in mind eq.(1), we see that the shift of the second resonance should be zero. This shift, however, is non zero and negative due to the finite thickness of the spike and second order effects [1]. On the other hand, the upper limit, $\Delta E_1 \approx \Delta E_{12}$ is reached for $L = 30\mathring{A}$ (approximately 10 monolayers, thick continuous line) or $L/L_W = 0.2$. Now, the resonances correspond to a double quantum well, where each well is $L_W' = 60\mathring{A}$ thick.

An example of wavefunction mapping for the lowest and second quasi-bound state, given by the energy shift $\Delta E_i = E_i' - E_i$, as a function of the probe potential spike position, is shown in Fig.(1b) for the thick probe potentials case, $L/L_W = 0.2$. Two aspects are relevant:(i) the probability density mapping is possible for thick potential probes, as far as the potential heigh is below a critical value; and (ii), above a critical potential height the energy shifts, ΔE_i, as a function of spike position z_0 show pronounced singularities, related the fact that ΔE_i is comparable to ΔE_{12}. Therefore, the mapping of the envelope wave function is restricted to situations where $\Delta E_i < \Delta E_{12}$, i.e., to the left of the crossover shown in the example of Fig.2: for $H = V_b$ and $L_W = 150\mathring{A}$, this crossover occurs at $L \approx 12\mathring{A}$, indicating an upper limit, $\Delta E_1 \approx 18meV$ for the energy shifts that still can be associated to a reliable wavefunction mapping.

A diagram indicating a parameter region for such reliable mapping for the lowest state is given in the inset of Fig.2. Here, ΔE_i ,at the crossover described in Fig. 2, is depicted as a function of a normalized perturbation strength, HL/L_W. The appropriate parameter region for a wavefunction mapping is the one below the straight line in the figure. This linear behaviour indicates a scalling of the energy shifts with the perturbation strength. Energy shifts up to $\Delta E_i \approx 35meV$ can be achieved, which could be resolved in experimental I-V characteristics of usual double-barrier diodes.

However, the main point from such a toy model calculation is that wide perturbative spikes, up to $L/L_W = 0.2$, still lead to reliable wave function imaging, an important generalization of eq.(1). This one dimensional result help to understand that extense potential bumps (provided that they are low enough) induced by AFM, indeed probe the wave functions in mesoscopic systems. In what follows we will be able to extend this result in a

simulation of the wave function mapping inside an open quantum dot.

III. IMAGING OF WAVE FUNCTIONS IN OPEN QUANTUM DOTS

A. Model calculation

The transmission probabilities through an open quantum dot are calculated within a Green's function formalism applied to a lattice model in the tight-binding approximation. This method has already been described throughout the literature and has been applied in a variety of problems in the context of mesoscopic systems [18–20]. For the sake of clarity this method is briefly sketched below.

The open quantum dot structure, emulated by a tight-binding lattice model is depicted in Fig.3(a). The black circles represent the lattice sites that define a square quantum dot conected to two dimensional contacts to the left and to the right by point contacts. The size of the quantum dot is $S_{QD} = 15a \times 15a$, where a is the host lattice parameter. The circles inside a square represent a potential column simulating the perturbation induced, for instance, by an AFM tip located on the sample at that position. In what follows we consider perturbations of a single host lattice site, which corresponds to a extension relative to the quantum dot are of $S_P \approx 4.5 \times 10^{-3} S_{QD}$, up to a 5×5 column, corresponding a relative extension of $S_P \approx 0.1 S_{QD}$.

It should be kept in mind that lattice models, with nearest neighbor interactions only, are usually thought as simple, although useful, approximations for superlattices or arrays of quantum dots, where each quantum well or quantum dot is represented by a site of the lattice, respectively. Apart from this extreme lattice limit, lattice models are also useful in emulating the bottom of semiconductor conduction bands that are well described by the effective mass approximation. In the present work, the tight-binding hopping parameter is chosen in order to emulate the electronic effective mass for the GaAs bottom of the conduction band, $m^* = 0.067 m_0$. Since, $V_{x,y} = -\hbar^2/(2m^* a^2)$, $V_{x,y} = 0.142$ eV for a lattice parameter of $a = 20$ Å. Such parametrization represents quantum dots with lateral sizes up to $L_D = 300 \mathring{A}$, Fig.3(a), still an order of magnitude lower than the typical dimensions of actual quantum dots constructed by litographic methods. However, the present results have the intention of illustrating the probing of the local probability density and the relevant scale is the ratio between the extension of the perturbative spike and the dot dimension, S_P/S_{QD}.

The AFM tip can also be seen as a controllable impurity in a quantum dot and therefore a simple tunable

experimental realization of a multiply connected nanostructure [17]. In the present approach, a continuous system is discretized into a tight-binding lattice, considering a single s-like orbital per site and only nearest-neighbour hopping elements. These two parameters are the only ones necessary for describing the electronic behaviour in lateraly modulated heterostructures near the bottom of the GaAs conduction band. The device region of a Open Quantum dot system modeled this way, Fig. 3(a), is $M = 45$ sites long and $N = 25$ sites wide. The total Hamiltonian, H_T, is a sum of four terms: the dot and the two point contacts regions, described by the H_D, and the left and rigth contact regions, H_L and H_R, respectively, and the coupling term between the contacts and the dot structure, V:

$$H_T = H_D + H_L + H_R + V \qquad (2)$$

We are interested in the transmission, $t_{\nu,\nu'}$, and reflexion, $r_{\nu,\nu'}$, amplitudes, related to the $G^+(\nu', r, \nu, l, E)$ and $G^+(\nu', l, \nu, l, E)$ Green's functions, respectively. Here, $l(r)$ stands for a sites column at the left(rigth) of the OQD device, as indicated in Fig.3(a); while $\nu(\nu')$ are transverse incident(scattered) modes in the contacts at a given energy E. The first step is calculating the Green's functions of the semi infinite contacts, C_L and C_R:

$$G^+(E) = \sum_{\nu,\mu} \frac{|\psi^{\nu\mu} >< \psi^{\nu\mu}|}{E - E^{\nu\mu} + i\eta}, \qquad (3)$$

where $|\psi^{\nu\mu}>$ and $E^{\nu\mu}$ are the eigenstates and eigenvalues of the contact regions, with $\nu(\mu)$ as transverse(longitudinal) quantum numbers. Actually, we need the matrix elements of the Green's functions for the l and r sites columns, given by:

$$G_{l(r)}(n, n') = \sum_{\nu=1}^{N} \chi_n^\nu (\chi_{n'}^\nu)^* \frac{e^{i\theta_\nu}}{|V_x|}; \qquad (4)$$

with

$$\theta_\nu = cos^{-1}[\frac{(E - \epsilon_\nu)}{2V_x} + 1] \qquad (5)$$

and

$$\chi_n^\nu = \sqrt{\frac{2}{N+1}} sin(\frac{\pi \nu n}{N+1}) \qquad (6)$$

The device region can be decoupled in M transverse chains with N sites each. The Hamiltonian for one of these chains, i, is written as:

$$H_i = \sum_{n=1}^{N} (|i, n > \epsilon_{in} < i, n|$$

$$+|i, n > V_{n,n+1} < i, n+1| + |i, n > V_{n,n-1} < i, n-1|), \qquad (7)$$

where the hopping elements at the edges are $V_{N,N+1} = V_{1,0} = 0$. The corresponding Green's function is:

$$G_i = [(E + i\eta)\mathbf{I} - H_i]^{-1} \qquad (8)$$

The Green's functions $G^+(\nu', r, \nu, l, E)$ and $G^+(\nu', l, \nu, l, E)$ are calculated by means of a recursive procedure, coupling the Green's functions of successive transversal chains along the device, eq.(8), based on the Dyson equation

$$G = G_0 + G_0 V G = G_0 + G V G_0 \qquad (9)$$

The starting point of this iterative procedure is the Green's function, given by eq.(4), corresponding to a transversal chain at the right, $r = M + 1$ (G_r), of the open quantum dot structure, successively coupled to the device chains, G_i, and finally to the left contact, G_l.

The transmited and reflected amplitudes are:

$$t_{\nu\nu'}(E) = i2|V_x|\sqrt{sin\theta_{\nu'} sin\theta_\nu}e^{i(\theta_{\nu l} - \theta_{\nu' r})}G^+(\nu', r, \nu, l, E) \qquad (10)$$

and

$$r_{\nu\nu'}(E) = i\sqrt{\frac{sin\theta_{\nu'}}{sin\theta_\nu}}e^{i(\theta_\nu + \theta_{\nu'})l}$$

$$\times[2|V_x|sin\theta_\nu G^+(\nu', l, \nu, l, E) + i\delta_{\nu'\nu}] \qquad (11)$$

The total transmission probability, the quantity discussed in what follows, is given by the Landauer-Büttiker formula:

$$T(E) = \sum_{\nu'}^{N}(\sum_{\nu}^{N}|t_{\nu'\nu}(E)|^2) \qquad (12)$$

B. Numerical Results: energy shifts and imaging

The main limitations of resonant tunneling mapping of the wave function, namely the broadness of measuread I-V characteristics, as well as the uncertainties related with a procedure involving a set of different samples, can be overcomed in the imaging of quasi-bound states in open quantum dots. The embeded potential spikes are substituted by the potential bumps induced by a AFM tip scanned over a single sample and the resonant tunneling current, a rather wide integration of transmission probability resonances, is reduced to single and well defined conductance peaks. Although imaging of coherent electron flow through a quantum point contact has been reported [8], where the mapping is achieved by measuring deviations of the quantized conductance plateaus as a function of AFM tip position, it remains to be properly discussed the use of energy shifts of conductance peaks to image the wave function inside a quantum dot.

Typical transmission probabilities as function of incident energy are shown in Fig.3(b). Here we clearly see two resonances due to quasi-bound states in the quantum dot below the threshold of the first quantized conductance plateau due to the quantum point contacts that connect the dot to the left and right two-dimensional reservoirs. The thin continuous line is for the unperturbed quantum dot. The other curves are for a potential bumps at the center of the dot with $H = 0.05eV$, but different sizes. It should be noticed that this is actually a strong perturbation, since the energy separation between the two resonances in the bare dot is $\approx 0.01eV$. The dashed line is for a delta function like bump, with $L = 1$. It can be seen that a small shift occurs for the lowest resonance, while the second one remains unchanged as expexted. The long dashed curve is for a wider bump, $L = 3$, with corresponding larger shifts of the resonances. The thick continuous line is for $L = 5$ revealing the signature of a doublet resonance of a symmetrically structured dot, instead of slightly single quantum dot perturbed levels. A clear analogy to the double barrier structure, Fig. 1(a), can be established.

The mapping of the probability density is obtained by scanning the potential bump across the quantum dot in both directions. This procedure introduces asymmetries in the structure as far as the perturbation is not at center of the structure, but the figure of merit is the position in energy of the transmission resonances and not the peak heigths. For the strength of the perturbation in the results shown in Fig. 3(b), the mentioned analogy with the results in Fig. 1(a) should be taken carefully. Indeed, such a high perturbation potential, $H = 50meV$, strongly affects the transmission channels when placed near the quantum point contacts. This is illustrated in Fig. 4, where the energy shifts of the lowest and second resonances are depicted as a function of the position of two different perturbative bumps. Fig. 4(a) represents a bona fide mapping of the probability densities for a very low, although spatially extended, perturbation: $H = 5meV$ and $L = 5a$; while Fig. 4(b) shows a inadequate mapping for $H = 50meV$ and $L = 3a$. The cusps in Fig. 4(b) are artifacts due to mode couplings and show no resemblance with the actual shapes of probability densities maxima, while the behavior of the energy shifts in Fig. 4(a) are qualitatively in agreement with the probability densities for the two lowest states of the unperturbed system.

The differences between a fair and a inadequate mapping situations become clearer by looking at the contour plots of the energy shifts as a function of the probing potential position, Fig. 5, for the same cases shown in Fig. 4. In Fig. 5(a) we see a fair mapping for quasi bound states in an open quantum dot with a high probability density leaking into the quantum point contacts.

This is not the case in Fig. 5(b), where the heigh of the potential bump, positioned near the quantum point contacts, strongly suppresses the resonant tunneling channels, turning the open system into a closed one. An appropriate mapping is also obtained for a even wider, $L = 7a$, low potential bump ($H = 5meV$) (not shown here). The interesting point here is that the lateral size of the perturbative bump is almost the half of the lateral size of the quantum dot been probed, corresponding to a bump to dot areas ratio of $S_P \approx 0.2S_{QD}$. Therefore, also for a two dimensional probability density mapping, the upper limit for the spatial extension of the probing potential is not crucial, as far as the corresponding heigh of the potential is kept low enough.

C. Tunable Fano resonances

As pointed out in the introduction, if a wave function mapping could be experimentally achieved, the open quantum dot system coupled to an AFM tip would be a realization of a tunable Fano system. Fano resonances have been observed in electronic transport through a quantum dot [11], but a completely tunable resonance has been reached only with the quantum dot in an Aharonov-Bohm interferometer [12]. The variation of the connecting channels, achievable by changing gate voltages may provide a partial tunability [11], but an extra degree of freedom, introduced by the movable AFM tip, allows such tuning in the absence of magnetic field effects.

Asymmetric Fano line shapes are the result of the interference between a resonant and non-resonant scattering paths. For weakly coupled states, the line shapes of the associated resonances are Lorentzian like. This is the case of the resonances shown in Fig. 3(b). However, when such a resonance occurs at energies near the onset of a conductance plateau, the line shape of the transmision resonance may change to a Fano like one. This changing the resonance line shape is illustrated in Fig.6, for a similar open quantum dot as shown previously (now $S_{QD} = 7a \times 7a$). Fig. 6(a) and Fig. 6(b) are for perturbative bumps at the positions indicated in the insets. It can be seen that the third resonance occurs at an energy where the transmission probability through the point contacts can not be neglected as in the case for the lower ones. Such contribution can be changed with gate voltages that tune the conection between the dot and the 2D reservoirs [11,21], with a corresponding modification of the resonance line shape.

Fig. 6 illustrates how an extra degree of fredom, introduced by the potential spike, keeping the quantum point contacts fixed, leads to the change from a Lorentzian to a Fano-like resonance. We believe that such an extra degree of freedom may permit a complete tunability of Fano resonances in open quantum dot sytems in absence of magnetic fields.

IV. FINAL REMARKS

The present work addresses the modeling of wave functions imaging by means of experimental perturbative approaches. The spectroscopy proposed is based on resonant tunneling. First we analyse a one dimensional problem, a resonant tunneling diode, closely related to the initial experimental proposals [1], relying on multiple samples experiments. The second situation studied here concerns a two dimensional problem, namely an open quantum dot in the resonant tunneling regime.

A remarkable analogy between both situations is established, with an important common result: wavefunction mapping is achievable with rather spatially extended perturbative potentials. This is in oposition to the initial supositions of delta like perturbative spikes [1,2], but provide a strong support to the imaging using AFM induced perturbations, where the exact form and extension of the depletion underneath the tip are not so clearly controled. We believe that our results open new possibilities to the imaging experiments carried out so far on single quantum point contacts [8]. An open quantum dot coupled to the tip of an AFM could also be a new realization of tunable resonance line shapes of the conductance through mesoscopic systems.

V. ACKNOWLEDGMENTS

[1] J-Y. Marzin and J-M. Gérard, Phys. Rev. Lett. **62**, 217 (1989).
[2] G. Salis *et al.*, Phys. Rev. Lett. **79**, 5106 (1997).
[3] G. Yang, J. K. Furdyna, and H. Luo, Phys. Rev. B **62**, 4226 (2000).
[4] A. Nogueira and A. Latgé, Phys. Rev. B **57**, 1649 (1998).
[5] E. E. Vdovin *et al.*, Science **290**, 122 (2000).
[6] S. G. Lemay *et al.*, NATURE **412**, 617 (2001).
[7] M. F. Crommie *et al.*, Science **262**, 218 (1993).
[8] M. A. Topinka *et al.*, Science **289**, 2323 (2000).
[9] G-P. He, S-L. Zhu, and Z. D. Wang, Phys. Rev. B **65**, 205321 (2002).
[10] A. R. Rocha and J. A. Brum, Braz. J. Phys. **32-2A**, 296 (2002).
[11] J. Göres, D. Goldhaber-Gordon, S. Heemeyer, M. A. Kastner, H. Shtrikman, D. Mahalu, and U. Meirav, Phys. Rev. B **62**, 2188 (2000).
[12] K. Kobayashi, H. Aikawa, S. Katsumoto, and Y. Iye, Phys. Rev. Lett. **88**, 256806 (2002).

[13] C. S. Kim, A. M. Satanin, Y. S. Joe, and R. M. Cosby, Phys. Rev. B **60**, 10962 (1999).

[14] P. J. Price, Superlattices Microstruc. **2**, 213 (1986). These results can also be obtained analytically for the present situation of zero bias, see H. Yamamoto and X. B. Zhao, Phys. Stat. Sol. (b) **217**, 793 (2000).

[15] S. Adachi, J. Appl. Phys. **58**, R1 (1985). $\Gamma - X$ coulping has not to be taken into account [16], since the X minimum related quasi-bound state are well above the states of interest. The double-barrier potential profile, considering the conduction band Γ minimum ,is illustrated in the inset of Fig.1(a). The effective masses are given by $m^* = (0.067 + 0.083x)m_0$ [15] and conduction-band offsets by $V_b = 860x$ meV [16].

[16] M. Rossmanith *et al.*, Phys. Rev. B **44**, 3168 (1991).

[17] Y. S. Joe, R. M. Cosby, M. W. C. Dharma-Wardana, and S. E. Ulloa, J. Appl. Phys. **76**, 4676 (1994).

[18] David K. Ferry and Stephen M. Goodnick, *Transport in Nanostructures* (Campbridge University Press, 1997), p. 156.

[19] F. Sols, M. Macucci, U. Ravaioli, and K. Hess, J. Appl. Phys. **66**, 3892 (1989).

[20] S. Datta, Superlattices and Microstructures, **28**, 253 (2000).

[21] S-J Xiong and Y. Yin, Phys. Rev. B **66**, 153315 (2002).

FIG. 1. (a) Examples of transmission probabilities, as a function of electron incident energy, for the structure shown in the inset with $z = L_W/2$, $H = V_b$; and $L = 0$ (continuos line), $L = 3\mathring{A}$ (dashed line), $L = 10\mathring{A}$ (long dashed), and $L = 30\mathring{A}$ (thick continuos line). Inset: double-barrier potential profile with an embeded perturbative barrier. (b) Energy shifts for the first (left) and second (rigth) resonances of the structure in (a) as a function of the position, z, of the perturbative barrier for $L = 30\mathring{A}$, for three different perturbative barrier height: $H = 0.043$ eV (lower curves), $H = 0.172$ eV (intermediate curves) and $H = 0.674$ eV (upper curves).
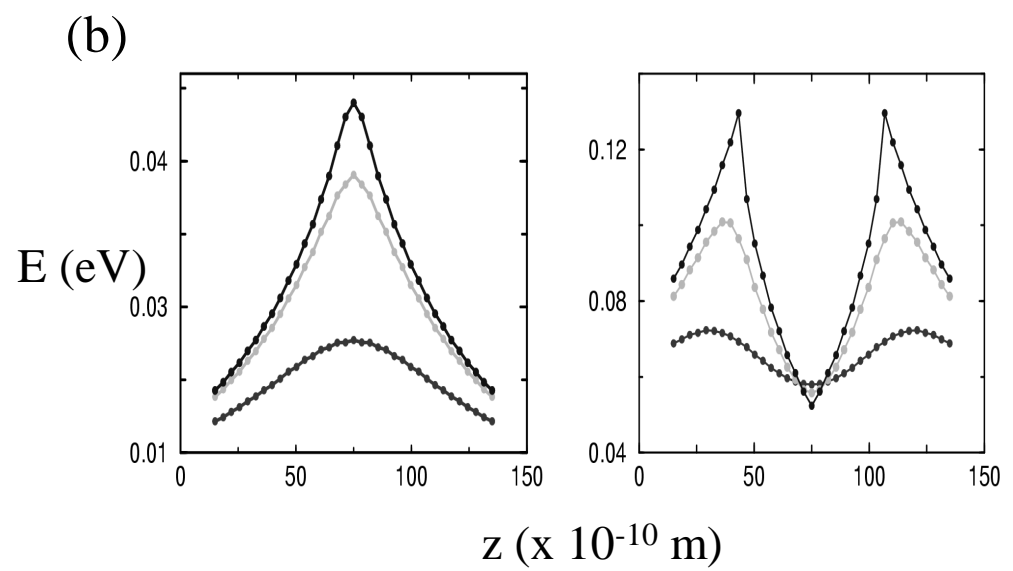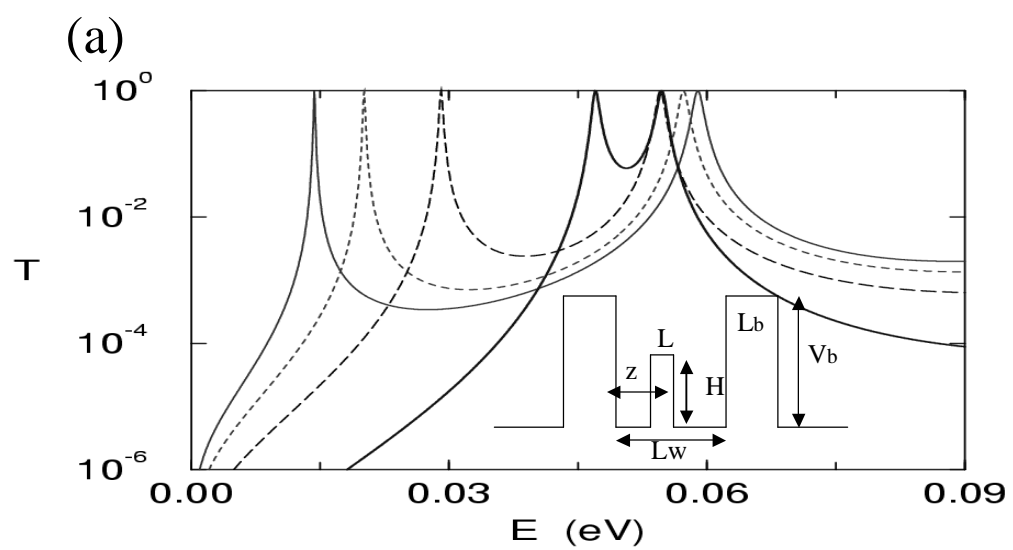
FIG. 2. Energy shift, $E_1' - E_1$, of the lowest quasi-bound state ; and the energy separation, $E_2 - E_1$, between the lowest and second bound states in a double-barrier structure, as a function of the perturbative barrier thickness, L. The perturbative barrier is located at the center of the well with $H = V_b$. The other parameters are the same as in Fig. 1. Inset: energy shift $\Delta E = E_1' - E_1$ at crossovers, as a function of the perturbation strength, HL/L_W.
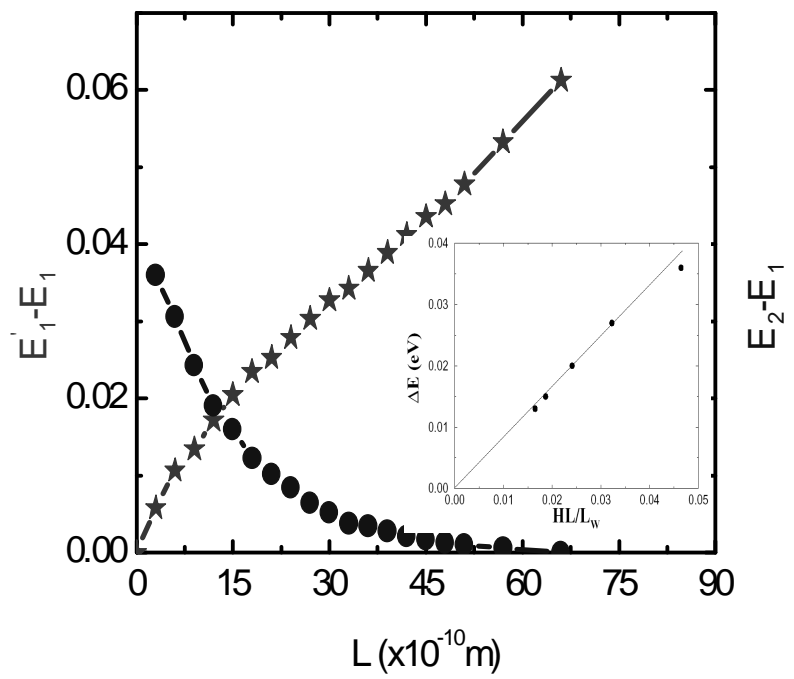
FIG. 3. (a) Schematic illustration of the open quantum dot structure. (b) Total transmission probabilities as function of incident energy for the structure in (a): bare structure (thin solid line), with a potential bump at the center of the structure with $H = 0.05$ eV and $L = 1a$ (dashed line), $L = 3a$ (long dashed line) and $L = 5a$ (thick solid line).
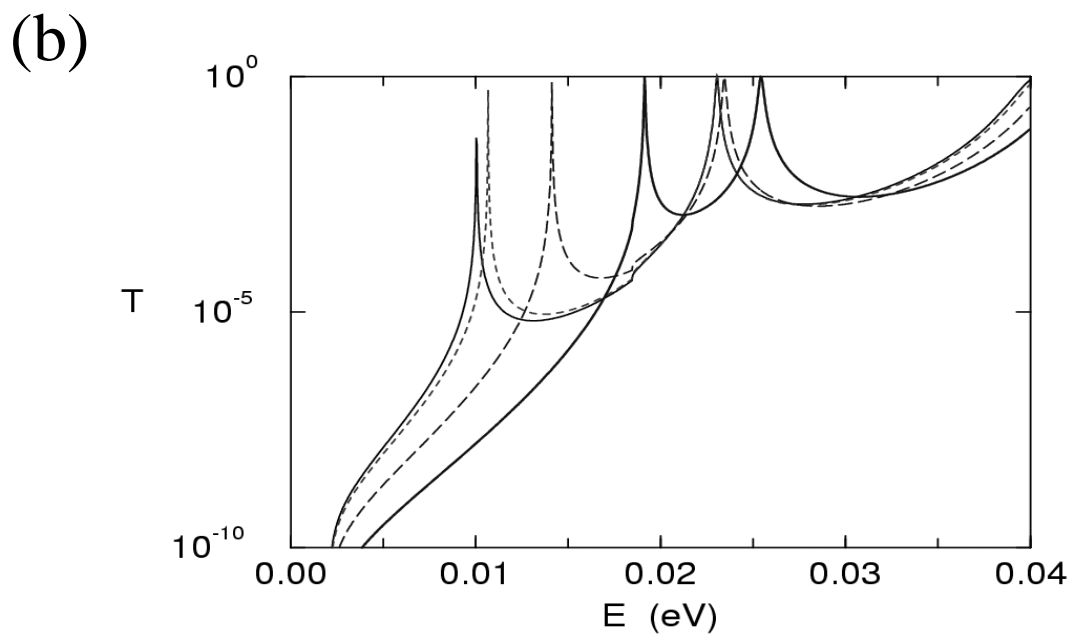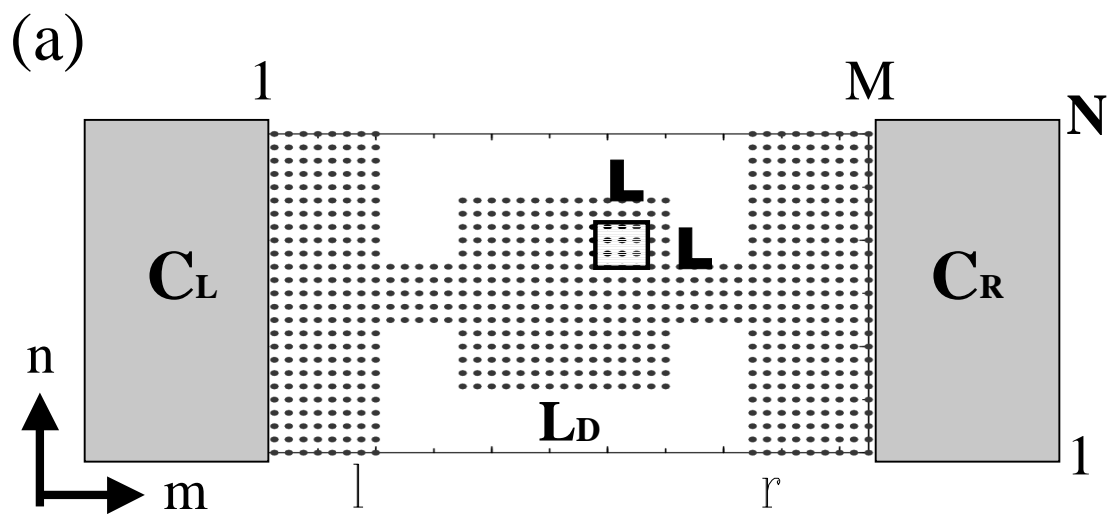
FIG. 4. Energy shifts of the lowest (left) and second (rigth) quasi bound states as a function of the position of the potential bump inside the open quantum dot structure. (a) Bona fide probability density mapping for a wide and low probe potential: $H = 5$ meV and $L = 5a$. (b) Unrealistic mapping for a high probe potential: $H = 50$ meV and $L = 3a$.

FIG. 5. Contour plots of energy shifts, corresponding to the situations depicted in Fig.4. The structure probed is an open quantum dot one and in (a), corresponding to a bona fide mapping, the contours indicate finite probability density in the contact regions. (b) high probe potentials isolate the quantum dot.
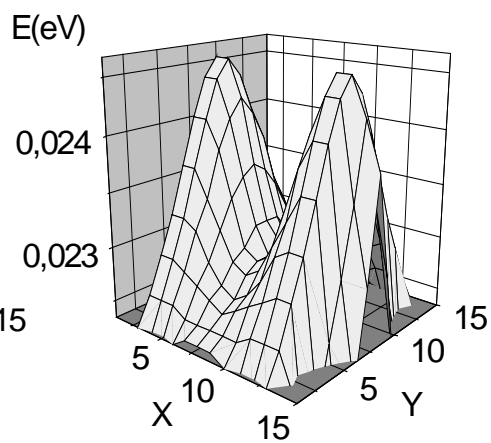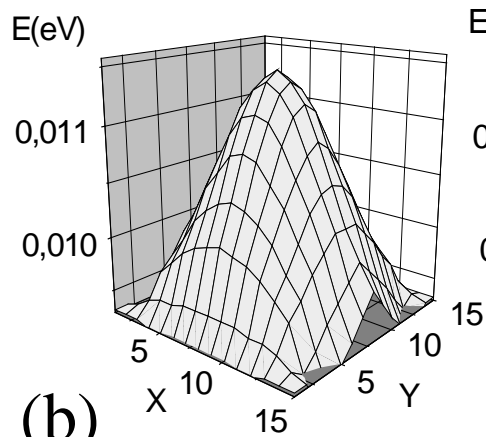
FIG. 6. Tuning of the resonance at the conductance plateau onset with varying tip position: (a) Breit-Wigner like resonance, and (b), Fano-like resonance.

(a)

(b)

E (eV)

z (x 10⁻¹⁰ m)

Y-axes: $E_1^{'} - E_1$ (left), $E_2 - E_1$ (right)

X-axis: $L \ (\times 10^{-10} m)$

Inset — Y-axis: $\Delta E \ (eV)$, X-axis: HL/L_W

(a)

1   M   N

C_L L   L C_R

n

m   l L_D r   1

(b)

(a)

(b)

(a)

(b)